This is a preprint, the final version is subject to change, of the American Mineralogist (MSA)
Cite as Authors (Year) Title. American Mineralogist, in press.
(DOI will not work until issue is live.) DOI: http://dx.doi.org/10.2138/am-2016-5332

Revision 1

Phase relations on the K_2CO_3-$CaCO_3$-$MgCO_3$ join at 6 GPa and 900-1400 °C: implication for incipient melting in carbonated mantle domains

Anton Shatskiy[1,2*], Konstantin D. Litasov[1,2], Yuri N. Palyanov[1,2], Eiji Ohtani[1,3]

[1]V.S. Sobolev Institute of Geology and Mineralogy, Russian Academy of Science, Siberian Branch, Novosibirsk 630090, Russia

[2]Novosibirsk State University, Novosibirsk 630090, Russia

[3]Department of Earth and Planetary Material Science, Tohoku University, Sendai 980-8578, Japan

*telephone/fax: +7 (382)-330-75-01, e-mail: anton.antonshatskiy.shatskiy@gmail.com

Abstract

In order to constrain the ternary K_2CO_3-$CaCO_3$-$MgCO_3$ *T-X* diagram at 6 GPa to expand upon the known K-Mg, K-Ca, and Ca-Mg binary systems we have carried out multi-anvil experiments along the K_2CO_3-$Ca_{0.5}Mg_{0.5}CO_3$ join. The diagram has primary phase fields for K_2CO_3, $K_2Mg(CO_3)_2$, $K_2Ca_{0.1\text{-}0.5}Mg_{0.9\text{-}0.5}(CO_3)_2$, $K_4CaMg(CO_3)_4$, Ca-magnesite, and dolomite. The system has two liquidus minima near 1000 °C. At one minimum, a liquid with the composition of $36K_2CO_3{\cdot}64(Ca_{0.65}Mg_{0.35})CO_3$ is in equilibrium with three phases: Ca-magnesite, $K_2Ca_{0.1\text{-}0.5}Mg_{0.9\text{-}0.5}(CO_3)_2$ and $K_6Ca_2(CO_3)_5$. The other minimum, a liquid with the composition of $62K_2CO_3{\cdot}38Ca_{0.72}Mg_{0.28}CO_3$ is in equilibrium with K_2CO_3, $K_4CaMg(CO_3)_4$, and $K_6Ca_2(CO_3)_5$. At 900 °C, the ternary diagram contains two- and three-phase regions with Ca-magnesite, aragonite, $K_2Ca_3(CO_3)_4$, $K_2Ca(CO_3)_2$, $K_6Ca_2(CO_3)_5$, K_2CO_3, $K_2Ca_{0.1\text{-}0.5}Mg_{0.9\text{-}0.5}(CO_3)_2$ solid solution, $K_2Mg_{0.9}Ca_{0.1}(CO_3)_2$, and $K_4CaMg(CO_3)_4$. We also expect an existence of primary phase fields for $K_6Ca_2(CO_3)_5$, $K_2Ca_3(CO_3)_4$ and aragonite.

We suggest that extraction of K from silicate to carbonate components should decrease the minimum melting temperature of dry carbonated mantle rocks up to 1000 °C at 6 GPa and yield ultrapotassic Ca-rich dolomite melt containing more than 10 mol% K_2CO_3. As temperature increases above 1200 °C the melt evolves toward an alkali-poor, dolomitic liquid if the bulk molar CaO/MgO ratio > 1, or toward K-Mg-rich carbonatite if bulk CaO/MgO < 1. The majority of compositions of carbonatite inclusions in diamonds from around the world fall within the magnesite primary field between the 1300 and 1400 °C isotherms. These melts could be formed by partial melting of magnesite-bearing peridotite or eclogite with bulk Ca/Mg < 1 at temperatures ≤ 1400 °C. A few compositions revealed in the Ebelyakh and Udachnaya diamonds (Yakutia) fall within the dolomite primary field close to the 1200 °C isotherm. These melts could be formed by partial melting of dolomite-bearing rocks, such as carbonated pelite or eclogite with bulk Ca/Mg > 1 at temperatures ≤ 1200 °C.

Introduction

Carbonates are one of the important classes of minerals controlling both the temperature of melting and the composition of partial melt in the oxidized mantle domains (Wyllie and Huang, 1975; Wallace and Green, 1988; Dalton and Presnall, 1998a; Hammouda, 2003; Dasgupta et al., 2004; Luth, 2006; Litasov and Ohtani, 2009; Litasov and Ohtani, 2010; Litasov, 2011; Litasov et al., 2013). Resulting carbonate-rich melts have been recognized as effective metasomatic agents to modify mantle geochemical characteristics (Green and Wallace, 1988; Haggerty, 1989; Yaxley et al., 1991; Sweeney et al., 1995; Walter et al., 2008; Dasgupta et al., 2009; Hammouda et al., 2009). These melts could also be responsible for diamond formation in the lithospheric mantle (Akaishi et al., 1990; Kanda et al., 1990; Pal'yanov et al., 1999a; Pal'yanov et al., 1999b; Shatskii et al., 2002; Palyanov et al., 2007). The characteristic of mantle carbonate-rich melts is high-alkali contents, particularly K. This follows from the study of carbonatite melt inclusions in "fibrous" diamonds containing up to 15-20 mol% K_2O (Schrauder and Navon, 1994; Zedgenizov

et al., 2007; Klein-BenDavid et al., 2009) and high-pressure experiments on partial melting of carbonated peridotites (Thibault et al., 1992; Brey et al., 2011), pelites (Grassi and Schmidt, 2011), and kimberlites (Yamashita et al., 1998; Ulmer and Sweeney, 2002).

High-pressure melting experiments in carbonated peridotite and pelite have shown that near solidus K-Ca-Mg-bearing melts are essentially carbonatitic in composition, containing ≤ 1 mol% SiO_2 (Brey et al., 2011; Grassi and Schmidt, 2011). This suggests that the solidus temperatures and nature of the melt are controlled by carbonates stable in the subsolidus (Luth, 2006). It is, therefore, essential to know phase relations in the K_2CO_3-$CaCO_3$-$MgCO_3$ system. Since the important mantle processes involving carbonates such as kimberlite magma generation, mantle metasomatism and diamond formation have occurred at the base of lithospheric mantle (150-230 km depths); 6 GPa pressure and temperatures exceeding 900 °C are relevant experimental conditions to study given system. In order to constrain the ternary K_2CO_3-$CaCO_3$-$MgCO_3$ *T-X* diagram at 6 GPa in addition to the known K_2CO_3-$MgCO_3$ (Shatskiy et al., 2013), K_2CO_3-$CaCO_3$ (Shatskiy et al., 2015a) and $CaCO_3$-$MgCO_3$ (Buob et al., 2006) systems in present study we have carried out experiments along the K_2CO_3-$Ca_{0.5}Mg_{0.5}CO_3$ join at temperatures between 900 and 1200 °C.

Experimental procedure

The study of phase relations along the K_2CO_3-$Ca_{0.5}Mg_{0.5}CO_3$ join was carried out at 6 GPa and 900-1200 °C using Kawai-type multianvil apparatuses equipped with DIA and wedge-type guide blocks at Tohoku University (Sendai, Japan) (Lloyd et al., 1963; Osugi et al., 1964; Shatskiy et al., 2011). We employed ZrO_2-based semisintered ceramics (OZ-8C) as a pressure medium with edge length of 20.5 mm and WC anvils with truncation edge length of 12 mm (Shatskiy et al., 2010; Shatskiy et al., 2013). Sample heating was achieved using a graphite heater, 4.5/4.0 mm in outer/inner diameter and 11 mm in length. Sample temperature was controlled using W-$Re_{3/25\%}$ thermocouple inserted in the heater center and electrically insulated

by Al_2O_3 tubes. The mixtures of synthetic K_2CO_3 and natural $CaMg(CO_3)_2$ dolomite from Brumado, Bahia, Brazil containing 0.3 mol% $FeCO_3$ were blended in an agate mortar under acetone and loaded into graphite cassettes (i.e., multiple sample holders). The Kawai cell assembly contained 16 cylindrical samples, 0.9 mm in diameter and 1.3 mm in length. Maximum radial and axial thermal gradients across the sample charges were found to be about 5 and 10 °C/mm, respectively (Shatskiy et al., 2013). Thereby each sample has higher-temperature (HT) and lower-temperature (LT) side. For this study we used 8 holes in two upper cassettes with different sample compositions shown in Tables 1-4. The remaining holes were employed to study an alternative carbonate system. Since K_2CO_3 is extremely hygroscopic material, special attention for sample preparation and loading was paid. The loaded cassettes were dried at 300 °C for 3–5 h and stored in a drying oven. Prepared assemblies were stored at 130 °C in a vacuum for ≥12 h prior to experiment. During opening the vacuum oven was filled with dry air.

All experiments were performed as follows. The assemblies were compressed at room temperature to 6.0 MN (600 ton) in a DIA press, or to 4.5 MN (450 ton) in a wedge press, corresponding to a pressure of 6 GPa. Then the samples were heated to temperatures ranging from 900 to 1200 °C for 13–36 h. The temperature was maintained within 0.5 °C of the desired value using the temperature controlling program (written by T. Katsura). The maximum temperature difference between samples inside the cassette and thermocouple value did not exceed 20 °C (Shatskiy et al., 2013). Experiments were terminated by shutting off the electrical power of the heater, followed by slow decompression.

Recovered samples were mounted into epoxy and polished in low-viscosity oil using 400-, 1000-, and 1500-mesh sandpapers and 3 μm diamond past. We used petroleum benzene to remove oil after polishing immediately prior to coating and loading the sample into a scanning electron microscope. Samples were studied using a Tescan MYRA 3 LMU scanning electron microscope coupled with an INCA energy-dispersive X-ray microanalysis system 450 equipped with the liquid nitrogen-free Large area EDS X-Max-80 Silicon Drift Detector (Oxford

Instruments) at IGM SB RAS (Novosibirsk, Russia). The EDS spectra were collected by rastering the electron beam over a surface area available for the analysis with linear dimensions from 10 to 300 μm at 20 kV accelerating voltage and 1 nA beam current. Counting times for spectra and X-ray elemental map collection were 20–30 s. No beam damage or change in measured composition with time was observed when using the current setting. We also confirmed that the size of the analyzed region has no measurable effect on the resulting data, as long as the area is significantly larger than the grain size. The EDS spectra were optimized for the quantification using standard XPP procedure included in the INCA Energy 450 software. The procedure of careful analysis of carbonates were described previously in details by (Shatskiy et al., 2013).

Experimental results

Selected backscattered electron (BSE) images of sample cross sections in the system K_2CO_3-$Ca_{0.5}Mg_{0.5}CO_3$ are shown in Figures 1 and 2. The chemical compositions of recovered carbonate phases are listed in Tables 1-4. The following arguments for equilibrium in our experiments can be provided. (1) In non-stoichiometric mixtures the limited reagents, i.e., K_2CO_3 at $X(K_2CO_3) < 50$ mol% and dolomite at $X(K_2CO_3) > 50$ mol% have been consumed completely. (2) Although minor amounts of dolomite were detected in aragonite+magnesite stability region at 900 °C and duration of 36 hours, no dolomite was observed after annealing at 900 °C for 38 hours and at 1000 °C and 29 hours duration. (3) In near stoichiometric mixture, $X(K_2CO_3) = 52$ mol%, both reagents, K_2CO_3 and $CaMg(CO_3)_2$, were completely consumed to form $K_4CaMg(CO_3)_4$ at 900 and 1000 °C. (4) All phases including solid solutions have uniform compositions and do not exhibit any zoning. This suggests that reactions have gone to completion and equilibrium has been achieved.

In run T2012 (900 °C, 36 h), the samples are represented by homogeneous aggregates of crystalline carbonates with grain size of 5-100 μm (Fig. 1a-d). No quenched products of melt

appeared in this experiment. In the starting mixtures with $X(K_2CO_3)$ = 91-62 mol% samples comprise of K_2CO_3 (K_2) and $K_4CaMg(CO_3)_2$ (Fig. 1a,b, Table 1). At $X(K_2CO_3)$ = 52 mol%, run products consist of $K_4CaMg(CO_3)_2$. At $X(K_2CO_3)$ = 42 mol%, most of the sample is represented by aggregate of $K_2Ca_{0.1}Mg_{0.9}(CO_3)_2$ and aragonite (Fig. 1c, Table 1). Aragonite was identified by Raman spectroscopy. The sample also contains relicts of dolomite, partially replaced by magnesite + aragonite assemblage (Fig. 1c,i). At $X(K_2CO_3) \geq$ 32 mol%, the samples contain $K_2Ca_{0.1}Mg_{0.9}(CO_3)_2$, Ca-bearing magnesite, aragonite, and relicts of dolomite (Fig. 1d, Table 1).

In run ES336 (1000 °C, 29 h), the LT side of samples with $X(K_2CO_3)$ = 91-62 mol% consists of K_2CO_3 and $K_2(Ca,Mg)(CO_3)_2$ (Fig. 1e-g). The latter phase changes its composition from $K_2Ca_{0.3}Mg_{0.7}(CO_3)_2$ to $K_2Ca_{0.5}Mg_{0.5}(CO_3)_2$ with $X(K_2CO_3)$ increasing from 91 to 62 mol% (Table 2). Thin layer of dendritic aggregate at the HT side indicates partial melting (Fig. 1e-g). At $X(K_2CO_3)$ = 91, 77, and 62 mol%, the melt pools adjoin the layers of K_2CO_3 (Fig. 1e), K_2CO_3 + $K_2Ca_{0.4}Mg_{0.6}(CO_3)_2$ (Fig. 1f), and $K_2Ca_{0.5}Mg_{0.5}(CO_3)_2$ (Fig. 1g), respectively. At $X(K_2CO_3)$ = 52 mol%, the sample consists of $K_2Ca_{0.5}Mg_{0.5}(CO_3)_2$ and does not contain quenched melt (Table 2). At $X(K_2CO_3)$ = 42 mol%, the melt pool adjoins the $K_2Ca_{0.3}Mg_{0.7}(CO_3)_2$ layer (Fig. 1h). Besides, the LT side of this sample contains aragonite (Fig. 1h). At $X(K_2CO_3)$ = 32 mol%, the melt contacts with the $K_2(Ca_{0.1}Mg_{0.9})(CO_3)_2$ layer, containing minor amounts of Ca-bearing magnesite (Fig. 1j). The LT side of the sample with $X(K_2CO_3)$ = 32 mol% is represented by the $K_2(Ca_{0.1}Mg_{0.9})(CO_3)_2$ + Ca-magnesite + aragonite assemblage (Fig. 1j). At $X(K_2CO_3)$ = 22 and 11 mol%, the melt contacts with the magnesite-aragonite layer (Fig. 1k,l). Besides, the LT side contains $K_2Ca_{0.1}Mg_{0.9}(CO_3)_2$ (Fig. 1k,l).

In run T2013 (1100 °C, 17 h), the samples with $X(K_2CO_3)$ = 91 and 77 mol% consist of K_2CO_3 in the LT side and quenched melt at the HT side (Fig. 2a, Table 3). At $X(K_2CO_3)$ = 62 mol%, the sample underwent complete melting (Table 3). At $X(K_2CO_3)$ = 52 and 42 mol% the sample contains $K_2Ca_{0.15}Mg_{0.85}(CO_3)_2$ in addition to quenched melt (Table 3). The melts are slightly enriched in $CaCO_3$ relative to the starting compositions (Table 3). At $X(K_2CO_3)$ = 32

mol%, the sample consists of quenched melt and Ca-magnesite (Fig. 2b). At $X(K_2CO_3)$ = 22 and 11 mol%, the samples consist of quenched melt, Ca-magnesite and dolomite (Fig. 2c,d, Table 3).

In run ES337 (1200 °C, 13 h), the samples with $X(K_2CO_3)$ = 91 and 77 mol% consist of K_2CO_3 at the LT side and quenched melt at the HT side (Fig. 2e,f, Table 4). At $X(K_2CO_3)$ = 62 mol%, the sample is completely molten (Fig. 2g, Table 4). At $X(K_2CO_3)$ = 52 and 42 mol%, the samples contain $K_2Ca_{0.1}Mg_{0.9}(CO_3)_2$ and quenched melt (Fig. 2h,i). At $X(K_2CO_3)$ = 32 and 22 mol%, Ca-magnesite coexists with melt (Fig. 2j,k, Table 4). At $X(K_2CO_3)$ = 11 mol%, the LT side of sample consists of dolomite, whereas melt appears at the HT side. Besides, Ca-magnesite crystals appear at the dolomite-melt interface (Fig. 2l, Table 4).

Isothermal sections of the ternary K_2CO_3-$CaCO_3$-$MgCO_3$ system at 6 GPa are illustrated in Figure 3. At 900 °C, most of the area of the diagram is taken up by multiphase regions (Fig. 3a). There are three two-phase areas: K_2+$K_2(Ca,Mg)_{SS}$, Ca-Mgs+K_2Mg_{SS}, $K_2(Ca,Mg)_{SS}$+Arg and one three-phase Ca-Mgs+Arg+$K_2Mg_{0.9}Ca_{0.1}$ triangle. The area along the $CaCO_3$-K_2CO_3 side remains undetermined. Increasing the temperature to 1000 °C (Fig. 3b) gives rise to two melt fields. The melt field is surrounded by five two-phase fields: $K_2(Ca,Mg)_{SS}$+L, Ca-Mgs+L, Arg+L, K_2Ca_3+L, and K_6Ca_2+L and by five three-phase fields: $K_2Mg_{0.9}Ca_{0.1}$+Ca-Mgs+L, Mgs+Arg+L, Arg+K_2Ca_3+L, K_2Ca_3+K_6Ca_2+L, and K_6Ca_2+ $K_2Mg_{0.5}Ca_{0.5}$+L. The second melt field adjoins three two-phase fields: K_2 + L, $K_2Ca_{0.5}Mg_{0.5}$+L, K_6Ca_2 +L and three three-phase fields: K_2+$K_2Ca_{0.5}Mg_{0.5}$+L, $K_2Ca_{0.5}Mg_{0.5}$+K_6Ca_2 +L, and K_6Ca_2 +K_2+L. At 1100 °C and higher temperatures, the two melt fields merged into single one (Fig. 3c-f). At 1100 and 1200 °C, all major phases, Ca-Mgs, Dol_{SS}, Arg, K_2Ca_3, K_6Ca_2, and K_2, have a field of stability in the presence of liquid (Fig. 3c,d).

Near-liquidus phase relations in the K_2CO_3-$CaCO_3$-$MgCO_3$ system are illustrated in Figure 4. Within the K_2CO_3-$CaCO_3$-$MgCO_3$ join, we find primary phase fields for K_2, K_2Mg, $K_2(Ca,Mg)_{SS}$, K_4CaMg, Ca-Mgs, and Dol. We also expect an existence of primary phase fields for K_6Ca_2, K_2Ca_3 and Arg (Fig. 4). The system has two minima on the liquidus at about 1000 °C

(Fig. 3b, 4). These points resemble eutectics. One minimum is marked by the point A (Fig. 4). At this point, a liquid with composition of $36K_2CO_3 \cdot 64(Ca_{0.65}Mg_{0.35})CO_3$ is in equilibrium with tree phases. The two phases are Mgs and $K_2(Ca,Mg)$. The third phase is most probably K_6Ca_2. Another minimum is located at point B (Fig. 4), having the composition of $62K_2CO_3 \cdot 38Ca_{0.72}Mg_{0.28}CO_3$. At this point, a liquid is in equilibrium with K_2, K_4CaMg, and K_6Ca_2.

Discussion

Partial melting of K-bearing carbonated peridotite

Most studies of phase relations in carbonated peridotite under mantle conditions were conducted in K-poor systems (< 0.1 wt% K_2O) (e.g., Dalton and Presnall, 1998b; Dasgupta and Hirschmann, 2007; Brey et al., 2008; Keshav and Gudfinnsson, 2014). At the same time, potassium as incompatible element, which drastically reduces solidus temperature of carbonated systems (Litasov, 2011), would have pronounced effect on partial melting of carbonated mantle domains as well as on partial melt composition. Therefore, here we compare our experimental results in the K_2CO_3-$CaCO_3$-$MgCO_3$ system at 6 GPa with available experimental data on phase relations in K-bearing carbonated peridotite.

Ghosh et al. (2009) reported that the solidus temperature of K-bearing lherzolite (G09) with 5.9 mol% CO_2, 0.42 mol% Na_2O and 0.22 mol% K_2O is 1380 °C at 10 GPa, which is 120 °C lower than that reported by Dasgupta and Hirschmann (2006) for K-poor lherzolite (DH06) with 5.8 mol% CO_2, 0.24 mol% Na_2O and 0.01 mol% K_2O. In both studies the stable subsolidus assemblage includes olivine, two pyroxenes, garnet, and magnesite. The difference in solidus temperature could be related to the difference in the bulk $Na_2O/(Na_2O+CO_2)$ ratio, which decreases the solidus temperature of carbonated lherzolite (Dasgupta and Hirschmann, 2007). Yet, in the G09 peridotite bulk $Na_2O/(Na_2O+CO_2) = 6.6$, which is even lower than in the DH06 peridotite with $Na_2O/(Na_2O+CO_2) = 7.58$. Most probably the temperature difference is caused by

higher K content in G09 peridotite. However, the melting reaction remains unclear. The K deficits inferred by mass-balance calculations in subsolidus runs (Ghosh et al., 2009) imply the presence of additional K-rich phase. However, Ghosh et al. (2009) did not find the direct evidence of the host phase for K below the apparent solidus, which is likely due to its small volume fraction.

Brey et al. (2011) performed melting experiments in the systems lherzolite-K_2CO_3-$MgCO_3$ (LC) and harzburgite-K_2CO_3-$MgCO_3$ (HC) at pressures from 6 to 10 GPa (Table 5). It was found that an addition of K_2CO_3 to magnesite peridotite depresses the solidus from 1500 to 1200 °C at 10 GPa (Brey et al., 2008; Brey et al., 2011). In addition to olivine (Ol), pyroxenes, garnet (Grt) and magnesite (Mgs) the near solidus LC assemblage includes K-Mg carbonate, $K_2(Mg,Fe)(CO_3)_2$, at 8 and 10 GPa and anhydrous phase X, $K_2Mg_2Si_2O_7$, at 8 GPa. With increasing temperature from 1200 to 1400 °C the melt composition in the LC system evolves from [$42K_2CO_3 \cdot 58Ca_{0.1}Mg_{0.8}Fe_{0.1}CO_3$ + 1.1 mol% SiO_2] toward [$31K_2CO_3 \cdot 69Ca_{0.1}Mg_{0.7}Fe_{0.2}CO_3$ + 2.8 mol% SiO_2] (Table 6). In HC, the partial melt approaches to the [$11K_2CO_3 \cdot 89Ca_{0.25}Mg_{0.62}Fe_{0.13}CO_3$ + 11 mol% SiO_2] composition at 1400 °C and 6 GPa (Table 6). The difference in the LC and HC partial melt compositions is due to the difference in the bulk carbonate concentrations: 7.6 mol% K_2CO_3 + 12.4 mol% $MgCO_3$ in lherzolite and 1.5 mol% K_2CO_3 + 9.7 mol% $MgCO_3$ in harzburgite. It is obvious that above 1200°C the melt composition in LC is controlled by the near-eutectic carbonate mixture, $38K_2CO_3$+$62MgCO_3$, which is 20 mol% of entire system. Indeed, the compositions of partial melt in LC are broadly consistent with those on the K_2CO_3-$MgCO_3$ join (see Fig. 4 in Shatskiy et al. (2015b)). The bulk K_2CO_3 content in HC is substantially less than in LC. This limits K_2CO_3 concentration in the high-temperature (1400 °C) melt and reveals the effect of the Ca component.

Based on variations in melt fraction, Brey et al. (2011) concluded that the position of the LC and HC solidi are placed near 1100 °C at 6 GPa, which is about 100-150 °C lower than minimum melting temperatures of the $K_2(Mg,Fe)(CO_3)_2$ + $(Mg,Fe)CO_3$ assemblage (Shatskiy et

al., 2013; Shatskiy et al., 2015b). Furthermore, this assemblage coexists with the carbonate melt in LC at 10 GPa and 1262 °C, i.e., it cannot be responsible for the incipient melting. This must reflect the influence of the added Ca component, which can be extracted to carbonate via reaction:

$$2MgCO_3\ (Mgs) + CaMgSi_2O_6\ (CPx) = CaMg(CO_3)_2\ (Dol\ or\ L) + Mg_2Si_2O_6\ (OPx),$$

above 3-4 GPa (Brey et al., 1983; Dalton and Presnall, 1998b; Dasgupta and Hirschmann, 2007). According to our data on phase relations in the K_2CO_3-$CaCO_3$-$MgCO_3$ system, $K_2Mg(CO_3)_2$ and $MgCO_3$ can coexist with liquid phase at 6 GPa and 1000-1200 °C (Fig. 3b-d). Based on these data we suggest that the incipient melting of K-carbonated peridotite may occur at 1000 °C. At this temperature the near-solidus melt has K-Ca-dolomitic composition, $36K_2CO_3 \cdot 64Ca_{0.65}Mg_{0.35}CO_3$. With increasing temperature above 1200 °C the melt evolves toward K-Mg carbonatite similar to that reported by Brey et al. (2011) (Fig. 5, Table 6). The CaO/(CaO+MgO+FeO) ratio (Ca#) in the high-temperature melt would be controlled by the bulk $K_2O/(K_2O+CO_2)$ ratio. According to the experimental data (Dalton and Presnall, 1998a; Brey et al., 2011) the decrease of bulk $K_2O/(K_2O+CO_2)$ from 28 to 12 and 0 mol% is accompanied by an increase of the Ca# in the melt from 10 to 25 and 37 mol%, respectively, at 1400 °C and 6 GPa (Fig. 5).

Partial melting of K-bearing carbonated pelite

Marine sediments are believed to be an important carrier of volatiles, most notably CO_2, recycled back into the Earth's interior at subduction zones (Kerrick and Connolly, 2001; Dasgupta and Hirschmann, 2010). Computed phase equilibria of a selected set of sediment bulk compositions (Kerrick and Connolly, 2001) suggest that carbonate should remain stable in dehydrated sedimentary assemblages and enters the deeper parts of subduction zones, beyond sub-arc depths (Dasgupta and Hirschmann, 2010).

Grassi and Schmidt (2011) reported that at 5.5-8.5 GPa the solidus temperature of K-bearing carbonated pelite (DG2) remains nearly constant at about 1070 °C (Table 5). The

subsolidus assemblage consists of garnet (Grt), coesite (Coe), kyanite (Ky), clinopyroxene (CPx), K-feldspar (Kfs), and dolomite (Dol). Incipient melting occurs through the reaction:

$6KAlSi_3O_8$ (Kfs) + $6CaMg(CO_3)_2$·(Dol) → $2Al_2SiO_5$ (Ky) + $13SiO_2$ (Coe) + $Mg_3Al_2Si_3O_{12}$ (Grt) + 3[K_2CO_3·2$CaCO_3$·$MgCO_3$] (L).

Since potassium and Ca-Mg carbonate is the dominant contributors to the melting reaction in the carbonated pelite, it is of interest to compare these results with those in the silicate-free K_2CO_3-$CaCO_3$–$MgCO_3$ system, particularly in light of suggestions that the melting relationships in carbonate system strongly influence the solidus of carbonate-silicate systems (Yaxley and Brey, 2004; Dasgupta et al., 2005; Buob et al., 2006; Luth, 2006; Dasgupta and Hirschmann, 2007). The lowest degree melting at 8 GPa and 1100 °C of the DG2 carbonated pelite yields ultrapotassic carbonate melt [37$(K_{0.94}Na_{0.06})_2CO_3$·63$(Ca_{0.62}Mg_{0.16}Fe_{0.22})CO_3$ + 0.6 mol% SiO_2], which is close in composition to that in the K_2CO_3-$CaCO_3$-$MgCO_3$ system at 1000 °C and 6 GPa [36K_2CO_3·64$(Ca_{0.65}Mg_{0.35})CO_3$] (Fig. 3b, Table 6). The K_2CO_3 content in the melt rapidly decreases with increasing temperature and at 1180 °C and 5.5 GPa, the composition of the DG2 partial melt approaches to [14$(K_{0.74}Na_{0.26})_2CO_3$·86$(Ca_{0.58}Mg_{0.24}Fe_{0.18})CO_3$ + 6.2 mol% SiO_2], which is close to the partial melt in the K_2CO_3-$CaCO_3$-$MgCO_3$ system at 1200 °C and 6 GPa [16K_2CO_3·84$(Ca_{0.58}Mg_{0.42})CO_3$] (Fig. 3d, Table 6). Although melting in the K-bearing carbonated pelite and K_2CO_3-$CaCO_3$-$MgCO_3$ systems is controlled by different subsolidus assemblages: Dol + Kfs and Dol + $K_2Mg(CO_3)_2$, respectively, in both cases the partial melts evolves along the same compositional trend with increasing temperature (Fig. 5).

Implications for the origin of carbonatitic melts entrapped by fibrous diamonds

The composition of melts/fluids in the metasomatized subcratonic mantle has been well documented through the study of microinclusions in cubic fibrous diamonds, the fibrous coats of coated octahedral diamonds and in clouds within octahedral diamonds worldwide (Navon, 1991; Logvinova et al., 2008). The composition of the melts/fluids varies between three end-members: a carbonatitic end-member enriched in Mg, Fe, Ca, K and CO_3^{2-}; a hydrous-silicic end-member

enriched in Si, Al, K and H_2O; and a hydrous-saline fluid enriched in Cl, K, Na and H_2O (Navon, 1991; Schrauder and Navon, 1994; Izraeli et al., 2001; 2004; Klein-BenDavid et al., 2004; Zedgenizov et al., 2004; Klein-BenDavid et al., 2006; Tomlinson et al., 2006; Klein-BenDavid et al., 2007; Zedgenizov et al., 2007; Logvinova et al., 2008; Klein-BenDavid et al., 2009; Weiss et al., 2009; Zedgenizov et al., 2009; Logvinova et al., 2011; Zedgenizov et al., 2011). The compositions of carbonatite melt microinclusions in fibrous diamonds worldwide in comparison with the liquidus isotherms in the K_2CO_3-$MgCO_3$-$CaCO_3$ system at 6 GPa are shown in Figure 6. The silica content and molar $H_2O/(CO_2+H_2O)$ ratio in the selected compositions vary from 5 to 15 mol% and from 0.01 to 0.4 mol%, respectively. When plotted on a (K_2O,Na_2O)–(MgO,FeO)–CaO triangle, the majority of compositions fall within the magnesite primary field between the 1300–1400 °C isotherms (Fig. 6). This interval corresponds to an upper estimate of the entrapment temperatures. Presence of Fe and Na components would shift the liquidus surface to lower temperatures resulting in underestimation of the entrapment temperatures. However, their maximum contribution would not exceed several tens of degrees Celsius (Cooper et al., 1975; Shatskiy et al., 2014; Shatskiy et al., 2015a; Shatskiy et al., 2015b). These melts could be formed by partial melting of magnesite-bearing peridotites or eclogites with the bulk molar Ca/Mg ratio < 1 at temperatures ≤ 1400 °C. A few compositions revealed in the Ebelyakh and Udachnaya diamonds (from Yakutia localities) (Zedgenizov et al., 2007; Zedgenizov et al., 2011) fall in the dolomite primary field and plot on the 1200 °C isotherm (Fig. 6). These melts could be formed by partial melting of the dolomite-bearing rocks, such as carbonated pelites or eclogites with the bulk molar Ca/Mg ratio > 1 at temperatures ≤ 1200 °C. Note that carbonatite inclusions in the Ebelyakh diamonds have systematically higher Ca# ranging from 40 to 70 mol% (Zedgenizov et al., 2011), which may suggest a distinct source region (Fig. 6). The diamonds from other localities reveal the carbonatite melts with the Ca# varying from 40 to 20 mol% (Fig. 6) (Schrauder and Navon, 1994; Tomlinson et al., 2006; Zedgenizov et al., 2007; Klein-BenDavid et al., 2009; Weiss et al., 2009; Zedgenizov et al., 2009). The alkali content,

$(K_2O+Na_2O)/(K_2O+Na_2O+CaO+MgO+FeO)$, generally falls in the range of 35-10 mol% (Fig. 6). The compositions of carbonatite inclusions in fibrous diamonds are in a good agreement with the compositional trends for evolution of carbonatite partial melts with temperature revealed from the experiments in the K_2CO_3-$MgCO_3$-$CaCO_3$ and carbonate-silicate systems (Brey et al., 2011; Grassi and Schmidt, 2011) (Fig. 5, 6).

Conclusions

The ternary K_2CO_3-$CaCO_3$-$MgCO_3$ *T-X* diagram at 6 GPa has been constrained using the known K_2CO_3-$MgCO_3$ (Shatskiy et al., 2013), K_2CO_3-$CaCO_3$ (Shatskiy et al., 2015a) and $CaCO_3$-$MgCO_3$ (Buob et al., 2006) diagrams and our new data on phase relations along the K_2CO_3-$Ca_{0.5}Mg_{0.5}CO_3$ join.

The system has two minima on the liquidus near 1000 °C. At one minimum, a liquid with the composition of $36K_2CO_3{\cdot}64(Ca_{0.65}Mg_{0.35})CO_3$ is in equilibrium with three phases: Ca-magnesite, $K_2Ca_{0.1\text{-}0.5}Mg_{0.9\text{-}0.5}(CO_3)_2$ and $K_6Ca_2(CO_3)_5$. At another minimum, a liquid with the composition of $62K_2CO_3{\cdot}38Ca_{0.72}Mg_{0.28}CO_3$ is in equilibrium with K_2CO_3, $K_4CaMg(CO_3)_4$, and $K_6Ca_2(CO_3)_5$. The diagram has primary phase fields for K_2CO_3, $K_2Mg(CO_3)_2$, $K_2Ca_{0.1\text{-}0.5}Mg_{0.9\text{-}0.5}(CO_3)_2$, $K_4CaMg(CO_3)_4$, Ca-magnesite, and dolomite. We also expect an existence of primary phase fields for $K_6Ca_2(CO_3)_5$, $K_2Ca_3(CO_3)_4$ and aragonite.

We suggest that under anhydrous conditions extraction of K from silicate to carbonate components decreases the minimum melting temperature of carbonated mantle rocks up to 1000 °C at 6 GPa and yields ultrapotassic Ca-rich dolomite or dolomite-ankerite melt containing more than 10 mol% K_2CO_3. With temperature increase above 1200 °C the melt evolves toward alkali-poor dolomitic if bulk CaO/MgO > 1, or toward K-Mg-rich carbonatite if bulk CaO/MgO < 1.

Nomenclature

Mgs - magnesite; Ca-Mgs - Ca-bearing magnesite; Arg - aragonite; Dol_{SS} - $(Ca,Mg)CO_3$; K_2 - K_2CO_3; K_2Mg - $K_2Mg(CO_3)_2$; $K_2(Ca,Mg)_{SS}$ - $K_2Ca_{0.1\text{-}0.5}Mg_{0.5\text{-}0.9}(CO_3)_2$ solid solution; K_4CaMg - $K_4CaMg(CO_3)_4$; K_6Ca_2 - $K_6Ca_2(CO_3)_5$; K_2Ca - $K_2Ca(CO_3)_2$, K_2Ca_3 - $K_2Ca_3(CO_3)_4$; Per - periclase.

Acknowledgements

We thank anonymous referee for constructive comments, Don Baker and Keith Putirka for editorial handling. This work was supported by the Russian Scientific Fund (proposal no. 29 14-17-00609) and performed under the project of the Ministry of Education and Science of Russian Federation (no. 14.B25.31.0032).

Figure captions

Fig. 1. Representative BSE images of sample cross-sections illustrating phase relations along the K_2CO_3-$Ca_{0.5}Mg_{0.5}CO_3$ join at 6 GPa and 900-1000 °C. K_2 = K_2CO_3; K_2Mg = $K_2Ca_xMg_{1-x}(CO_3)_2$, where x ~ 0.1; $K_2(Ca,Mg)$ = $K_2Ca_xMg_{1-x}(CO_3)_2$, where x = 0.3-0.5; Dol = dolomite; Mgs = Ca-bearing magnesite; Arg = aragonite; L = liquid. Scale bar length is 300 μm.

Fig. 2. Representative BSE images of sample cross-sections illustrating phase relations along the K_2CO_3-$Ca_{0.5}Mg_{0.5}CO_3$ join at 6 GPa and 1100-1200 °C. K_2 = K_2CO_3; K_2Mg = $K_2Ca_xMg_{1-x}(CO_3)_2$, where x ~ 0.1; Dol = dolomite; Mgs = Ca-bearing magnesite; L = liquid. Scale bar length is 300 μm.

Fig. 3. Isobaric and isothermal sections in the ternary K_2CO_3-$MgCO_3$-$CaCO_3$ system at 900 °C (a), 1000 °C (b), 1100 °C (c), and 1200 °C (d) at 6 GPa. K_2 = K_2CO_3; K_2Mg = $K_2Ca_xMg_{1-x}(CO_3)_2$, where x ~ 0.1; $K_2(Ca,Mg)$ = $K_2Ca_xMg_{1-x}(CO_3)_2$, where x = 0.3-0.5; K_2Ca_3 = $K_2Ca_3(CO_3)_4$; K_2Ca = $K_2Ca(CO_3)_2$; K_6Ca_2 = $K_6Ca_2(CO_3)_5$; Dol = dolomite; Mgs = Ca-bearing magnesite; Arg = aragonite; L = liquid. Gray areas in squares denote relicts of initial compounds and phases observed in low-temperature end of the partially molten samples. Partial melt compositions in K-bearing carbonated pelite, GS11 = (Grassi and Schmidt, 2011), and K-bearing

carbonated lherzolite, B11 = (Brey et al., 2011) are shown for comparison. Boundaries are dashed when expected.

Fig. 4. Melting phase relations for the K_2CO_3-$MgCO_3$-$CaCO_3$ ternary at 6 GPa. Black lines (dashed where inferred) are boundary lines and white lines (dashed where inferred) are liquidus isotherms with temperatures in °C. K_2 = K_2CO_3; K_2Mg = $K_2Ca_xMg_{1-x}(CO_3)_2$, where x ~ 0.1; $K_2(Ca,Mg)_{SS}$ = $K_2Ca_xMg_{1-x}(CO_3)_2$, where x = 0.1-0.5; K_4CaMg = $K_4CaMg(CO_3)_4$; K_2Ca_3 = $K_2Ca_3(CO_3)_4$; K_2Ca = $K_2Ca(CO_3)_2$; K_6Ca_2 = $K_6Ca_2(CO_3)_5$; Dol = dolomite; Mgs = Ca-bearing magnesite; Arg = aragonite.

Fig. 5. Possible compositional trends of carbonatitic partial melts with increasing temperature at 6 GPa. The liquidus isotherms in the K_2CO_3-$MgCO_3$-$CaCO_3$ system at 6 GPa are shown by grey lines for comparison. DP98 = (Dalton and Presnall, 1998a), B11 = (Brey et al., 2011) and GS11 = (Grassi and Schmidt, 2011).

Fig. 6. Compositions of carbonatite melt microinclusions in diamonds worldwide in comparison with the liquidus isotherms in the K_2CO_3-$MgCO_3$-$CaCO_3$ system at 6 GPa. SN94 = fibrous diamonds with cubic morphology from Jwaneng, Botswana (Schrauder and Navon, 1994); W09 = coated octahedral diamonds from Kankan, Guinea (Weiss et al., 2009); T06 = coated octahedral diamonds from the Panda kimberlite, Canada (Tomlinson et al., 2006); Z07 = cuboid fibrous diamonds from the Udachnaya kimberlite, Russia (Zedgenizov et al., 2007); K09U, K09Z, K09Y, K09A = fibrous diamonds with cubic morphology from the Udachnaya, Zarnitsa, Yubileinaya, Aykhal kimberlite pipes, Russia (Klein-BenDavid et al., 2009); Z09 = cuboid diamonds with fibrous inner zone from Internationalnaya kimberlite, Russia (Zedgenizov et al., 2009); Z11 = fibrous diamonds with cubic and semirounded morphology from the Ebelyakh placers, northeastern Siberian Platform, Russia (Zedgenizov et al., 2011). Z = fibrous diamonds from Yubileinaya kimberlite, Russia (Zedgenizov et al., unpublished).

References

Akaishi, M., Kanda, H., and Yamaoka, S. (1990) Synthesis of diamond from graphite-carbonate systems under very high temperature and pressure. Journal of Crystal Growth, 104(2), 578-581.

Brey, G., Brice, W.R., Ellis, D.J., Green, D.H., Harris, K.L., and Ryabchikov, I.D. (1983) Pyroxene-carbonate reactions in the upper mantle. Earth and Planetary Science Letters, 62(1), 63-74.

Brey, G.P., Bulatov, V.K., Girnis, A.V., and Lahaye, Y. (2008) Experimental melting of carbonated peridotite at 6-10 GPa. Journal of Petrology, 49(4), 797-821.

Brey, G.P., Bulatov, V.K., and Girnis, A.V. (2011) Melting of K-rich carbonated peridotite at 6-10 GPa and the stability of K-phases in the upper mantle. Chemical Geology, 281(3-4), 333-342.

Buob, A., Luth, R.W., Schmidt, M.W., and Ulmer, P. (2006) Experiments on $CaCO_3$-$MgCO_3$ solid solutions at high pressure and temperature. American Mineralogist, 91(2-3), 435-440.

Dalton, J.A., and Presnall, D.C. (1998a) The continuum of primary carbonatitic-kimberlitic melt compositions in equilibrium with lherzolite: Data from the system CaO-MgO-Al_2O_3-SiO_2-CO_2 at 6 GPa. Journal of Petrology, 39(11-12), 1953-1964.

-. (1998b) Carbonatitic melts along the solidus of model lherzolite in the system CaO-MgO-Al_2O_3-SiO_2-CO_2 from 3 to 7 GPa. Contributions to Mineralogy and Petrology, 131(2-3), 123-135.

Dasgupta, R., Hirschmann, M.M., and Withers, A.C. (2004) Deep global cycling of carbon constrained by the solidus of anhydrous, carbonated eclogite under upper mantle conditions. Earth and Planetary Science Letters, 227(1-2), 73-85.

Dasgupta, R., Hirschmann, M.M., and Dellas, N. (2005) The effect of bulk composition on the solidus of carbonated eclogite from partial melting experiments at 3 GPa. Contributions to Mineralogy and Petrology, 149(3), 288-305.

Dasgupta, R., and Hirschmann, M.M. (2006) Melting in the Earth's deep upper mantle caused by carbon dioxide. Nature, 440(7084), 659-662.

Dasgupta, R., and Hirschmann, M.M. (2007) Effect of variable carbonate concentration on the solidus of mantle peridotite. American Mineralogist, 92(2-3), 370-379.

Dasgupta, R., Hirschmann, M.M., McDonough, W.F., Spiegelman, M., and Withers, A.C. (2009) Trace element partitioning between garnet lherzolite and carbonatite at 6.6 and 8.6 GPa with applications to the geochemistry of the mantle and of mantle-derived melts. Chemical Geology, 262(1-2), 57-77.

Dasgupta, R., and Hirschmann, M.M. (2010) The deep carbon cycle and melting in Earth's interior. Earth and Planetary Science Letters, 298(1-2), 1-13.

Ghosh, S., Ohtani, E., Litasov, K.D., and Terasaki, H. (2009) Solidus of carbonated peridotite from 10 to 20 GPa and origin of magnesiocarbonatite melt in the Earth's deep mantle. Chemical Geology, 262, 17-28.

Grassi, D., and Schmidt, M.W. (2011) The melting of carbonated pelites from 70 to 700 km depth. Journal of Petrology, 52(4), 765-789.

Green, D.H., and Wallace, M.E. (1988) Mantle metasomatism by ephemeral carbonatite melts. Nature, 336(6198), 459-462.

Haggerty, S.E. (1989) Mantle metasomes and the kinship between carbonatites and kimberlites. In K. Bell, Ed. Carbonatites: Genesis and Evolution, p. 546-560. Unwin Hyman Ltd, London.

Hammouda, T. (2003) High-pressure melting of carbonated eclogite and experimental constraints on carbon recycling and storage in the mantle. Earth and Planetary Science Letters, 214(1-2), 357-368.

Hammouda, T., Moine, B.N., Devidal, J.L., and Vincent, C. (2009) Trace element partitioning during partial melting of carbonated eclogites. Physics of the Earth and Planetary Interiors, 174(1-4), 60-69.

Izraeli, E.S., Harris, J.W., and Navon, O. (2001) Brine inclusions in diamonds: a new upper mantle fluid. Earth and Planetary Science Letters, 187(3-4), 323-332.

-. (2004) Fluid and mineral inclusions in cloudy diamonds from Koffiefontein, South Africa. Geochimica et Cosmochimica Acta, 68, 2561–2575.

Kanda, H., Akaishi, M., and Yamaoka, S. (1990) Morphology of synthetic diamonds grown from Na_2CO_3 solvent-catalyst. Journal of Crystal Growth, 106(2-3), 471-475.

Kerrick, D.M., and Connolly, J.A.D. (2001) Metamorphic devolatilization of subducted marine sediments and the transport of volatiles into the Earth's mantle. Nature, 411(6835), 293-296.

Keshav, S., and Gudfinnsson, G.H. (2014) Melting phase equilibria of model carbonated peridotite from 8 to 12 GPa in the system CaO-MgO-Al_2O_3-SiO_2-CO_2 and kimberlitic liquids in the Earth’s upper mantle. American Mineralogist, 99(5-6), 1119-1126.

Klein-BenDavid, O., Izraeli, E.S., Hauri, E., and Navon, O. (2004) Mantle fluid evolution - a tale of one diamond. Lithos, 77(1-4), 243-253.

Klein-BenDavid, O., Wirth, R., and Navon, O. (2006) TEM imaging and analysis of microinclusions in diamonds: A close look at diamond-growing fluids. American Mineralogist, 91(2-3), 353-365.

Klein-BenDavid, O., Izraeli, E.S., Hauri, E., and Navon, O. (2007) Fluid inclusions in diamonds from the Diavik mine, Canada and the evolution of diamond-forming fluids. Geochimica Et Cosmochimica Acta, 71(3), 723-744.

Klein-BenDavid, O., Logvinova, A.M., Schrauder, M., Spetius, Z.V., Weiss, Y., Hauri, E.H., Kaminsky, F.V., Sobolev, N.V., and Navon, O. (2009) High-Mg carbonatitic

microinclusions in some Yakutian diamonds - a new type of diamond-forming fluid. Lithos, 112(S2), 648-659.

Litasov, K.D., and Ohtani, E. (2009) Solidus and phase relations of carbonated peridotite in the system CaO-Al_2O_3-MgO-SiO_2-Na_2O-CO_2 to the lower mantle depths. Physics of the Earth and Planetary Interiors, 177(1-2), 46-58.

Litasov, K.D., and Ohtani, E. (2010) The solidus of carbonated eclogite in the system CaO-Al_2O_3-MgO-SiO_2-Na_2O-CO_2 to 32 GPa and carbonatite liquid in the deep mantle. Earth and Planetary Science Letters, 295(1-2), 115-126.

Litasov, K.D. (2011) Physicochemical conditions for melting in the Earth's mantle containing a C–O–H fluid (from experimental data). Russian Geology and Geophysics, 52, 475-492.

Litasov, K.D., Shatskiy, A., Ohtani, E., and Yaxley, G.M. (2013) The solidus of alkaline carbonatite in the deep mantle. Geology, 41(1), 79-82.

Lloyd, E.C., Johnson, D.P., and Hutton, U.O. (1963) Dual-wedge high-pressure appaeatus. Unated States Patent, 3,100,912.

Logvinova, A.M., Wirth, R., Fedorova, E.N., and Sobolev, N.V. (2008) Nanometre-sized mineral and fluid inclusions in cloudy Siberian diamonds: new insights on diamond formation. European Journal of Mineralogy, 20(3), 317-331.

Logvinova, A.M., Wirth, R., Tomilenko, A.A., Afanas'ev, V.P., and Sobolev, N.V. (2011) The phase composition of crystal-fluid nanoinclusions in alluvial diamonds in the northeastern Siberian Platform. Russian Geology and Geophysics, 52(11), 1286-1297.

Luth, R.W. (2006) Experimental study of the $CaMgSi_2O_6$-CO_2 system at 3-8 GPa. Contributions to Mineralogy and Petrology, 151(2), 141-157.

Navon, O. (1991) High internal pressure in diamond fluid inclusions determined by infrared absorption. Nature, 353(6346), 746-748.

Osugi, J., Shimizu, K., Inoue, K., and Yasunami, K. (1964) A compact cubic anvil high pressure apparatus. Review of Physical Chemistry of Japan, 34(1), 1-6.

Pal'yanov, Y.N., Sokol, A.G., Borzdov, Y.M., Khokhryakov, A.F., Shatsky, A.F., and Sobolev, N.V. (1999a) The diamond growth from Li_2CO_3, Na_2CO_3, K_2CO_3 and Cs_2CO_3 solvent-catalysts at P=7 GPa and T=1700-1750 ^oC. Diamond and Related Materials, 8(6), 1118-1124.

Pal'yanov, Y.N., Sokol, A.G., Borzdov, Y.M., Khokhryakov, A.F., and Sobolev, N.V. (1999b) Diamond formation from mantle carbonate fluids. Nature, 400(6743), 417-418.

Palyanov, Y.N., Shatsky, V.S., Sobolev, N.V., and Sokol, A.G. (2007) The role of mantle ultrapotassic fluids in diamond formation. Proceedings of the National Academy of Sciences of the United States of America, 104(22), 9122-9127.

Schrauder, M., and Navon, O. (1994) Hydrous and carbonatitic mantle fluids in fibrous diamonds from Jwaneng, Botswana. Geochimica Et Cosmochimica Acta, 58(2), 761-771.

Shatskii, A.F., Borzdov, Y.M., Sokol, A.G., and Pal'yanov, Y.N. (2002) Phase formation and diamond crystallization in carbon-bearing ultrapotassic carbonate-silicate systems. Geologiya I Geofizika, 43(10), 940-950.

Shatskiy, A., Litasov, K.D., Terasaki, H., Katsura, T., and Ohtani, E. (2010) Performance of semi-sintered ceramics as pressure-transmitting media up to 30 GPa. High Pressure Research, 30(3), 443-450.

Shatskiy, A., Katsura, T., Litasov, K.D., Shcherbakova, A.V., Borzdov, Y.M., Yamazaki, D., Yoneda, A., Ohtani, E., and Ito, E. (2011) High pressure generation using scaled-up Kawai-cell. Physics of the Earth and Planetary Interiors, 189(1-2), 92-108.

Shatskiy, A., Sharygin, I.S., Gavryushkin, P.N., Litasov, K.D., Borzdov, Y.M., Shcherbakova, A.V., Higo, Y., Funakoshi, K., Palyanov, Y.N., and Ohtani, E. (2013) The system K_2CO_3-$MgCO_3$ at 6 GPa and 900-1450 ºC. American Mineralogist, 98(8-9), 1593-1603.

Shatskiy, A., Borzdov, Y.M., Litasov, K.D., Sharygin, I.S., Palyanov, Y.N., and Ohtani, E. (2015a) Phase relationships in the system K_2CO_3-$CaCO_3$ at 6 GPa and 900-1450ºC. American Mineralogist, 100(1), 223-232.

Shatskiy, A., Litasov, K.D., Ohtani, E., Borzdov, Y.M., Khmelnicov, A.I., and Palyanov, Y.N. (2015b) Phase relations in the K_2CO_3-$FeCO_3$ and $MgCO_3$-$FeCO_3$ systems at 6 GPa and 900-1700 °C. European Journal of Mineralogy, 27, DOI: 10.1127/ejm/2015/0027-2452.

Sweeney, R.J., Prozesky, V., and Przybylowicz, W. (1995) Selected trace and minor element partitioning between peridotite minerals and carbonatite melts at 18-46 kb pressure. Geochimica Et Cosmochimica Acta, 59(18), 3671-3683.

Thibault, Y., Edgar, A.D., and Lloyd, F.E. (1992) Experimental investigation of melts from a carbonated phlogopite lherzolite: implications for metasomatism in the continental lithosphere. American Mineralogist, 77, 784-794.

Tomlinson, E.L., Jones, A.P., and Harris, J.W. (2006) Co-existing fluid and silicate inclusions in mantle diamond. Earth and Planetary Science Letters, 250(3-4), 581-595.

Ulmer, P., and Sweeney, R.J. (2002) Generation and differentiation of group II kimberlites: Constraints from a high-pressure experimental study to 10 GPa. Geochimica Et Cosmochimica Acta, 66(12), 2139-2153.

Wallace, M.E., and Green, D.H. (1988) An experimental determination of primary carbonatite magma composition. Nature, 335(6188), 343-346.

Walter, M.J., Bulanova, G.P., Armstrong, L.S., Keshav, S., Blundy, J.D., Gudfinnsson, G., Lord, O.T., Lennie, A.R., Clark, S.M., Smith, C.B., and Gobbo, L. (2008) Primary carbonatite melt from deeply subducted oceanic crust. Nature, 454(7204), 622-630.

Weiss, Y., Kessel, R., Griffin, W.L., Kiflawi, I., Klein-BenDavid, O., Bell, D.R., Harris, J.W., and Navon, O. (2009) A new model for the evolution of diamond-forming fluids: Evidence from microinclusion-bearing diamonds from Kankan, Guinea. Lithos, 112(S2), 660-674.

Wyllie, P.J., and Huang, W. (1975) Peridotite, kimberlite, and carbonatite explained in the system CaO-MgO-SiO_2-CO_2. Geology, 3, 621-624.

Yamashita, H., Arima, M., and Ohtani, E. (1998) Melting experiments of kimberlites compositions up to 9 GPa: Determination of melt compositions using aggregates of diamond grains. 7th International Kimberlite Conference, p. 977-979, Cape Town.

Yaxley, G.M., Crawford, A.J., and Green, D.H. (1991) Evidence for carbonatite metasomatism in spinel peridotite xenoliths from western Victoria, Australia. Earth and Planetary Science Letters, 107(2), 305-317.

Yaxley, G.M., and Brey, G.P. (2004) Phase relations of carbonate-bearing eclogite assemblages from 2.5 to 5.5 GPa: implications for petrogenesis of carbonatites. Contributions to Mineralogy and Petrology, 146(5), 606-619.

Zedgenizov, D.A., Kagi, H., Shatsky, V.S., and Sobolev, N.V. (2004) Carbonatitic melts in cuboid diamonds from Udachnaya kimberlite pipe (Yakutia): evidence from vibrational spectroscopy. Mineralogical Magazine, 68(1), 61-73.

Zedgenizov, D.A., Rege, S., Griffin, W.L., Kagi, H., and Shatsky, V.S. (2007) Composition of trapped fluids in cuboid fibrous diamonds from the Udachnaya kimberlite: LAM-ICPMS analysis. Chemical Geology, 240(1-2), 151-162.

Zedgenizov, D.A., Ragozin, A.L., Shatsky, V.S., Araujo, D., Griffin, W.L., and Kagi, H. (2009) Mg and Fe-rich carbonate-silicate high-density fluids in cuboid diamonds from the Internationalnaya kimberlite pipe (Yakutia). Lithos, 112(S2), 638-647.

Zedgenizov, D.A., Ragozin, A.L., Shatsky, V.S., Araujo, D., and Griffin, W.L. (2011) Fibrous diamonds from the placers of the northeastern Siberian Platform: carbonate and silicate crystallization media. Russian Geology and Geophysics, 52(11), 1298-1309.

Table 1. Compositions (mol%) of the run products in the system K_2CO_3-$Ca_{0.5}Mg_{0.5}CO_3$ recovered from run T2012 at 6 GPa and 900 °C with duration 36 h.

***X*(K_2CO_3), phases**	K_2#	σ	Ca#	σ	Mg#	σ
91 (system)	91		4.5		4.5	
K_2	99.8	2.2	0	2	0.2	0.3
$K_2Ca_{0.53}Mg_{0.47}$	48.0	1	27.3	2.8	24.7	2.1
80 (system)*	80		10		10	
K_2	99.9	1.3	0	1.4	0.1	0.3
$K_2Ca_{0.51}Mg_{0.49}$	49.2	4.9	25.8	2.8	25	5.1
77 (system)	77		11.5		11.5	
K_2	100	1.8	0	1.7	0	0.1
$K_2Ca_{0.50}Mg_{0.50}$	46.6	1.3	26.8	4.9	26.6	4.5
62 (system)	62		19		19	
K_2	-		-		-	
$K_2Ca_{0.50}Mg_{0.50}$	47.9	4.4	26.2	3.2	26.0	3.6
60 (system)*	60		20		20	
K_2	97.5	5.2	1.7	3.8	0.9	1.7
$K_2Ca_{0.50}Mg_{0.50}$	49.1	2.9	27.3	2.2	23.7	4.3
52 (system)	52		24		24	
$K_2Ca_{0.52}Mg_{0.48}$	48.7	1.9	26.7	3.4	24.6	2.1
42 (system)	42		29		29	
$K_2Ca_{0.11}Mg_{0.89}$	48.7	0.6	5.7	0.8	45.6	0.9
Ca-Mgs	0	0.1	5.9	0.4	94.1	0.5
Arg	3	1.5	93.9	2.8	3	1.4
Dol	0.4	0.1	51.5	1.1	48.1	1.1
32 (system)	32		34		34	
$K_2Ca_{0.10}Mg_{0.90}$	48.8	1	5.2	0.8	46	1.1
Ca-Mgs	0.2	0.1	4.9	0.8	95	0.8
Arg	1.3	0.6	98.4	0.8	0.3	0.4
Dol	0.2	0.1	51.6	0.7	48.1	0.8
22 (system)	22		39		39	
$K_2Ca_{0.10}Mg_{0.90}$	46.3	6.1	5.2	1.3	48.5	5.5
Ca-Mgs	0		5		95	
Arg	1.2	0.5	98.2	0.9	0.6	0.6
11 (system)	11		44.5		44.5	
$K_2Ca_{0.10}Mg_{0.90}$	49.3	1	4.9	0.9	45.8	1.1
Ca-Mgs	0.1	0.1	4.3	0.4	95.5	0.4
Arg	0.8	0.4	99.1	1.1	0.1	0.8
Dol	0.4	0.3	51.3	1.5	48.2	1.2

Notes: ***X*(K_2CO_3)** = K_2CO_3 content in the system; K_2#, Ca#, Mg# = contents of K_2CO_3, $CaCO_3$ and $MgCO_3$ in the system and in phases; σ = standard deviation; K_2 = K_2CO_3; $K_2Ca_xMg_{1-x}$ = $K_2Ca_xMg_{1-x}(CO_3)_2$; Arg = aragonite; Ca-Mgs = Ca-bearing magnesite. Dol = dolomite; * = run B1001 at 6 GPa and 900 °C with duration 38 h.

Table 2. Compositions (mol%) of the run products in the system K_2CO_3-$Ca_{0.5}Mg_{0.5}CO_3$ recovered from run ES336 at 6 GPa and 1000 °C with duration 29 h.

***X*(K_2CO_3), phases**	K_2#	σ	Ca#	σ	Mg#	σ
91 (system)	91		4.5		4.5	
K_2	99.3	1	0	0.6	0.7	0.4
$K_2Ca_{0.33}Mg_{0.67}$	48.5	0.7	16.9	0.9	34.6	1.2
L	61.5	1.3	27.6	1.4	11.0	0.1
77 (system)	77		11.5		11.5	
K_2	99.9	0.8	0	1.1	0	0.3
$K_2Ca_{0.41}Mg_{0.59}$	49	2	21.1	3.1	29.9	2.9
L	59.6	2.7	28.7	2	11.7	1
62 (system)	62		19		19	
K_2	99.4	0.6	0.4	0.4	0.2	0.5
$K_2Ca_{0.51}Mg_{0.49}$	46.9	0.9	27.3	1	25.8	1.1
L	63.6		27.0		9.5	
52 (system)	52		24		24	
$K_2Ca_{0.49}Mg_{0.51}$	52.9	2.3	23.2	3.8	23.9	2.9
42 (system)	42		29		29	
$K_2Ca_{0.28}Mg_{0.72}$	47.4	2.5	14.2	1.5	38.4	3
Arg	1	0.2	98.8	0.1	0.2	0.1
L	34.7	1.2	43.6	0.2	21.7	1.4
32 (system)	32		34		34	
$K_2Ca_{0.08}Mg_{0.92}$	48.1	1.4	3.9	1.1	48	1.7
Arg	1	0.3	98.5	0.5	0.5	0.2
Ca-Mgs	0.2	0	5.1	0.3	94.7	0.3
L	36.9	2.8	43.2	2.4	19.9	2.1
22 (system)	22		39		39	
$K_2Ca_{0.08}Mg_{0.92}$	48.9	0.4	4.1	0.7	47.1	0.6
Arg	1	0.3	98	1.1	1	0.7
Ca-Mgs	0.1	0.1	4.6	0.1	95.3	0.1
L	35.6		39.4		27.7	
11 (system)	11		44.5		44.5	
$K_2Ca_{0.09}Mg_{0.91}$	48.3	1.2	4.5	0.6	47.2	1.7
Arg	0.9	1	98.6	1.9	0.5	1
Ca-Mgs	0	0.1	4.8	0.6	95.2	0.6
L	+		+		+	

Notes: ***X*(K_2CO_3)** = K_2CO_3 content in the system; K_2#, Ca#, Mg# = contents of K_2CO_3, $CaCO_3$ and $MgCO_3$ in the system and in phases; σ = standard deviation; K_2 = K_2CO_3; $K_2Ca_xMg_{1-x}$ = $K_2Ca_xMg_{1-x}(CO_3)_2$; Arg = aragonite; Ca-Mgs = Ca-bearing magnesite; L = liquid.

Table 3. Compositions (mol%) of the run products in the system K_2CO_3-$Ca_{0.5}Mg_{0.5}CO_3$ recovered from run T2013 at 6 GPa and 1100 °C with duration 17 h.

***X*(K$_2$CO$_3$), phase**	K$_2$#	σ	Ca#	σ	Mg#	σ
91 (system)	91		4.5		4.5	
K_2	93.5	0.9	6	1.7	0.5	0.8
L	65.5		14.6		19.9	
77 (system)	77		11.5		11.5	
K_2	94.2	2.4	4.5	1.7	1.3	0.9
L	70		15.2		14.8	
62 (system)	62		19		19	
L	61.8	5.4	20.4	2.8	17.9	2.6
52 (system)	52		24		24	
$K_2Mg_{0.81}Ca_{0.19}$	49.7	0.8	9.4	1.3	40.9	1.5
L	55.7	0.6	24.6	0.5	19.7	1.1
42 (system)	42		29		29	
$K_2Ca_{0.09}Mg_{0.91}$	48.3	1.3	4.7	0.7	47.0	1.7
L	38.3		32.7		28.9	
32 (system)	32		34		34	
Ca-Mgs	0.1	0.1	10.2	0.5	89.7	0.5
L	33.1	2.0	38.8		28.1	
22 (system)	22		39		39	
Dol	0.1	0.2	51.6	0.5	48.3	0.7
Ca-Mgs	0	0	9.7	0.1	90.3	0.2
L	27.1	0.7	43.8	0.8	29.2	1.4
11 (system)	11		44.5		44.5	
Dol	0.1	0.1	51.8	0.9	48.1	0.9
Ca-Mgs	0.2	0.3	8.1	0.6	91.6	0.5
L	24.7	2.3	46.9	1.3	28.4	3.6

Notes: ***X*(K$_2$CO$_3$)** = K_2CO_3 content in the system; K$_2$#, Ca#, Mg# = contents of K_2CO_3, $CaCO_3$ and $MgCO_3$ in the system and in phases; σ = standard deviation; K_2 = K_2CO_3; $K_2Ca_xMg_{1-x}$ = $K_2Ca_xMg_{1-x}(CO_3)_2$; Dol = dolomite; Ca-Mgs = Ca-bearing magnesite; L = liquid.

Table 4. Compositions (mol%) of the run products in the system K_2CO_3-$Ca_{0.5}Mg_{0.5}CO_3$ recovered from run ES337 at 6 GPa and 1200 °C with duration 13 h.

***X*(K$_2$CO$_3$), phases**	K$_2$#	σ	Ca#	σ	Mg#	σ
91 (system)	91		4.5		4.5	
K_2	99.7	1.6	0	1.7	0.3	0.5
L	73.2	0	15.0	0.1	11.8	0.1
77 (system)	77		11.5		11.5	
K_2	100		0		0	
L	72.2	2.7	16	1.4	11.8	1.2
62 (system)	62		19		19	
$K_2Mg_{0.86}Ca_{0.14}$						
L	60.9	1.2	20.5	1.5	18.6	0.4
52 (system)	52		24		24	
$K_2Mg_{0.86}Ca_{0.14}$	50.3	1.6	6.8	0.8	42.8	1
L	45.2	0.3	30.8	1	23.9	0.7
42 (system)	42		29		29	
$K_2Mg_{0.89}Ca_{0.11}$	48	1.7	5.6	0.4	46.3	1.5
L	42.3		31.8		25.9	
32 (system)	32		34		34	
Ca-Mgs	0.1	0.2	4.8	0.1	95.1	0.3
L	31.8		36.6		31.6	
22 (system)	22		39		39	
Ca-Mgs	0	0.1	6.7	0.8	93.2	0.7
L	27.4	0.3	41.3	0.3	31.3	0.1
11 (system)	11		44.5		44.5	
Dol	0.3	0.2	49.9	1.5	49.9	1.6
Ca-Mgs	0.2	0.1	9.2	1.1	90.7	1
L	15.9	0.3	48.4	0.2	35.7	0.5

Notes: ***X*(K$_2$CO$_3$)** = K_2CO_3 content in the system; K$_2$#, Ca#, Mg# = contents of K_2CO_3, $CaCO_3$ and $MgCO_3$ in the system and in phases; σ = standard deviation; K_2 = K_2CO_3; $K_2Ca_xMg_{1-x}$ = $K_2Ca_xMg_{1-x}(CO_3)_2$; Dol = dolomite; Ca-Mgs = Ca-bearing magnesite; L = liquid.

Table 5. Compositions of the starting materials used in the experiments on melting phase relations in anhydrous K-bearing carbonated-lherzolite (LC), harzburgite (HC) (Brey et al., 2011) and pelite (DG2) (Grassi and Schmidt, 2011) at pressures near 6 GPa.

Ref.	B11				GS11	
System	Harzburgite HC		Lherzolite LC		Pelite DG2	
	wt%	mol%	wt%	mol%	wt%	mol%
SiO_2	43.4	36.58	36.3	31.24	54.63	58.80
TiO_2	0.01	0.01	0.15	0.10	0.63	0.52
Al_2O_3	2.51	1.26	3.25	1.67	20.23	13.01
Cr_2O_3	1.01	0.34	0.34	0.12		
FeO	6.57	4.69	6.14	4.48	4.86	4.43
MnO	0.1	0.07	0.1	0.07		
MgO	39.2	49.92	34.9	45.38	2.92	4.75
CaO	0.81	0.74	3.09	2.89	5.88	6.87
Na_2O	0.02	0.02	0.3	0.25	3.20	3.38
K_2O	1.4	0.76	6.83	3.80	2.21	1.54
CO_2	4.8	5.60	8.4	10.00	4.50	6.70
Ca#		1.34		5.48		42.81
Mg#		90.18		86.03		29.58
Fe#		8.48		8.49		27.62

Notes: Ca# = Ca/(Ca+Mg+Fe); Mg# = Mg/(Ca+Mg+Fe); Fe# = Fe/(Ca+Mg+Fe).

Table 6. Partial melt compositions (mol%) in K-bearing carbonated-lherzolite (LC), harzburgite (HC) (Brey et al., 2011) and pelite (DG2) (Grassi and Schmidt, 2011).

System	Peridotite, B11					Pelite, GS11	
	LC				HC	GD2	
P, GPa	6.0				6.0	8.0	5.5
T, °C	1200	1300	1400	1400	1400	1100	1180
SiO_2	1.14	5.70	5.38	2.81	11.03	0.54	6.0
TiO_2	0.09	0.36	0.27	0.42	0.28	3.74	3.5
Al_2O_3	0.07	0.33	0.27	0.12	0.38	1.92	2.9
Cr_2O_3	0.02	0.04	0.02	0.01	0.05		
FeO	6.01	6.73	8.41	12.14	9.82	13.26	13.9
MnO	0.20	0.24	0.27	0.36	0.35		
MgO	45.48	42.79	48.04	47.29	48.33	9.24	18.1
CaO	5.45	9.19	6.87	6.76	19.77	36.68	43.7
Na_2O	0.74	1.02	0.61	0.83	1.08	1.93	3.1
K_2O	40.80	33.61	29.86	29.26	8.91	32.69	8.8
Ca#	9.57	15.65	10.85	10.22	25.37	61.98	57.7
Mg#	79.87	72.88	75.87	71.44	62.03	15.61	23.9
Fe#	10.56	11.47	13.28	18.34	12.60	22.41	18.4
A	42.17	37.10	32.49	31.25	11.37	36.91	13.6
B	5.53	9.85	7.33	7.02	22.48	39.11	49.9
C	52.29	53.06	60.19	61.73	66.14	23.98	36.6

Notes: Ca# = Ca/(Ca+Mg+Fe)*100; Mg# = Mg/(Ca+Mg+Fe)*100; Fe# = Fe/(Ca+Mg+Fe)*100; A = (K_2O+Na_2O)/(K_2O+Na_2O+CaO+MgO+FeO)*100; B = CaO/(K_2O+Na_2O+CaO+MgO+FeO)*100; C = (MgO+FeO)/(K_2O+Na_2O+CaO+MgO+FeO)*100.

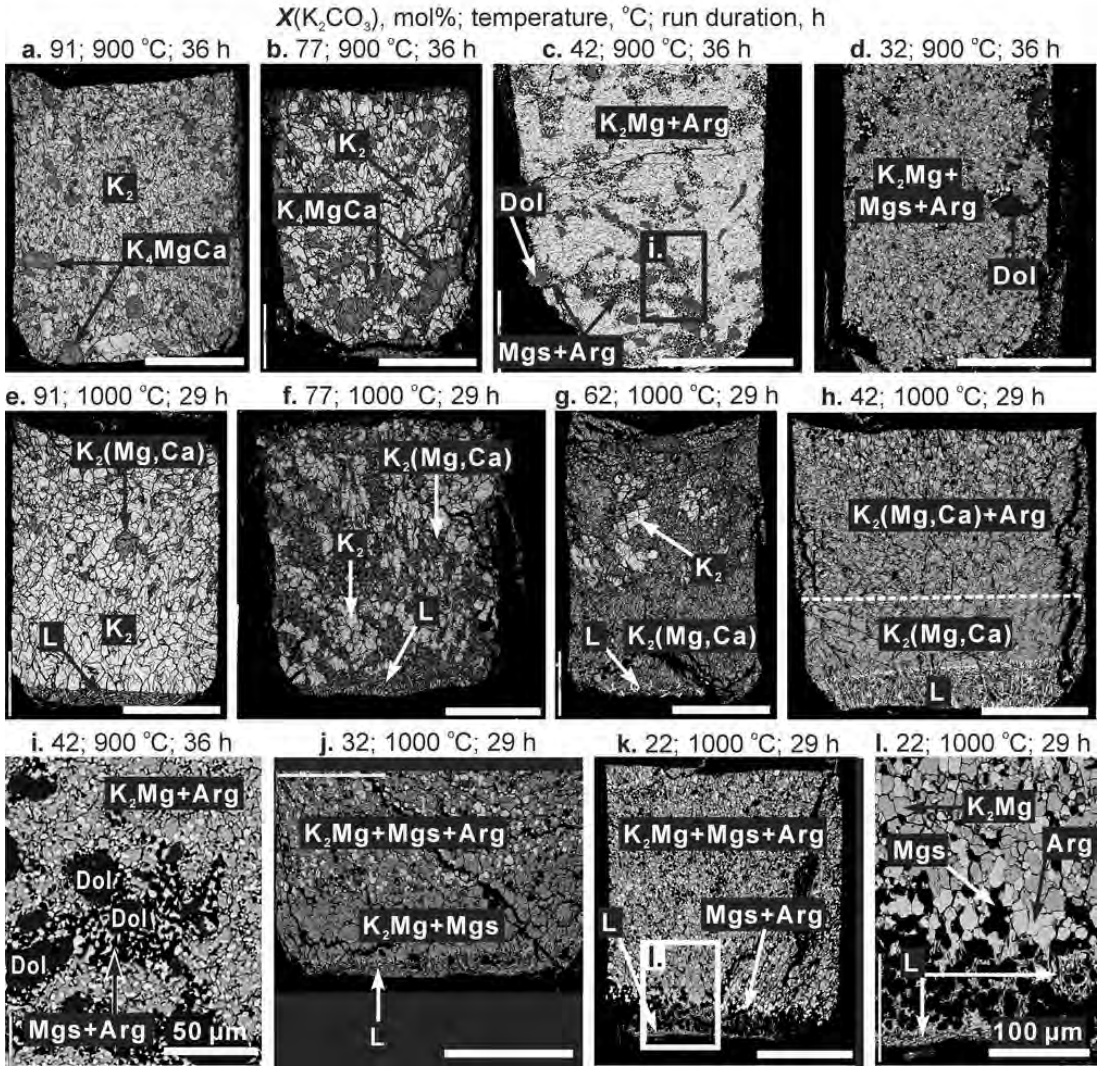
X(K2CO3), mol%; temperature, °C; run duration, h
a. 91; 900 °C; 36 h
b. 77; 900 °C; 36 h
c. 42; 900 °C; 36 h
d. 32; 900 °C; 36 h
K2
K4MgCa
K2
K4MgCa
K2Mg+Arg
Dol
i.
Mgs+Arg
K2Mg+
Mgs+Arg
Dol
e. 91; 1000 °C; 29 h
f. 77; 1000 °C; 29 h
g. 62; 1000 °C; 29 h
h. 42; 1000 °C; 29 h
K2(Mg,Ca)
L
K2
K2(Mg,Ca)
K2
L
K2
L
K2(Mg,Ca)
K2(Mg,Ca)+Arg
K2(Mg,Ca)
L
i. 42; 900 °C; 36 h
j. 32; 1000 °C; 29 h
k. 22; 1000 °C; 29 h
l. 22; 1000 °C; 29 h
K2Mg+Arg
Dol
Dol
Dol
Mgs+Arg
50 µm
K2Mg+Mgs+Arg
K2Mg+Mgs
L
K2Mg+Mgs+Arg
L
Mgs+Arg
i.
K2Mg
Mgs
Arg
L
100 µm

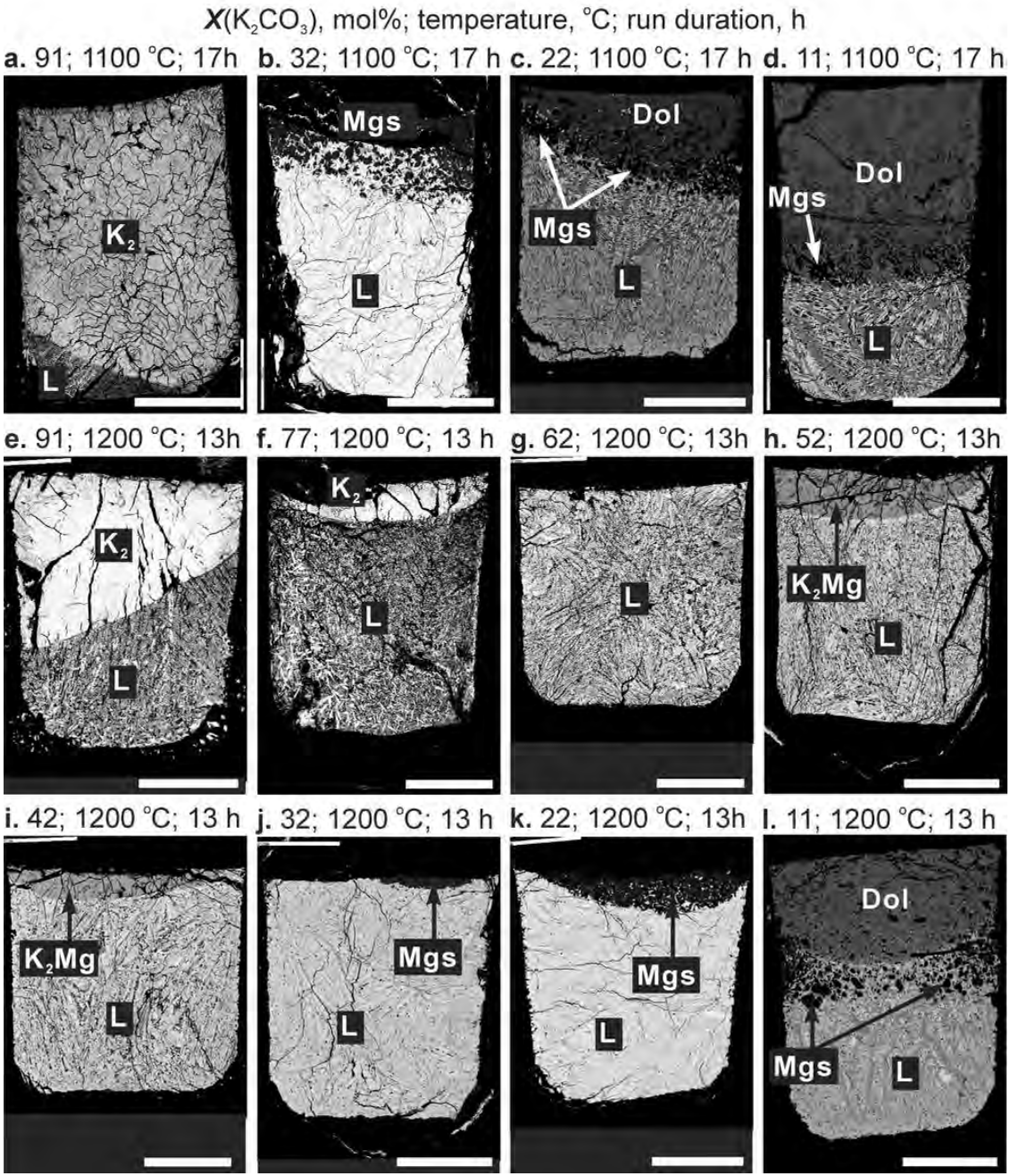
X(K2CO3), mol%; temperature, °C; run duration, h
a. 91; 1100 °C; 17h
b. 32; 1100 °C; 17 h
c. 22; 1100 °C; 17 h
d. 11; 1100 °C; 17 h
K2
L
Mgs
L
Dol
Mgs
L
Dol
Mgs
L
e. 91; 1200 °C; 13h
f. 77; 1200 °C; 13 h
g. 62; 1200 °C; 13h
h. 52; 1200 °C; 13h
K2
L
K2
L
L
K2Mg
L
i. 42; 1200 °C; 13 h
j. 32; 1200 °C; 13 h
k. 22; 1200 °C; 13h
l. 11; 1200 °C; 13 h
K2Mg
L
Mgs
L
Mgs
L
Dol
Mgs
L

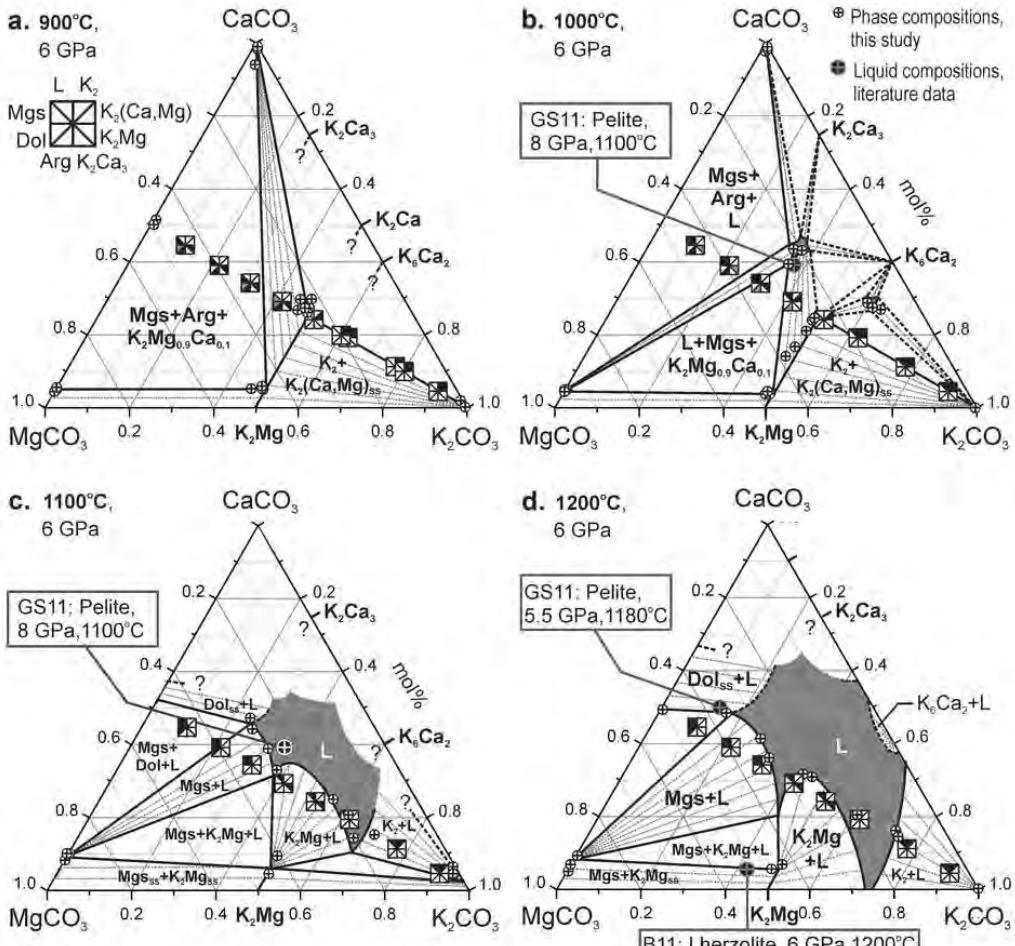
a. 900°C, 6 GPa
L K2
Mgs K2(Ca,Mg)
Dol K2Mg
Arg K2Ca3
CaCO3
MgCO3
K2CO3
K2Mg
K2Ca3
K2Ca
K6Ca2
Mgs+Arg+ K2Mg0.9Ca0.1
K2+ K2(Ca,Mg)ss
b. 1000°C, 6 GPa
Phase compositions, this study
Liquid compositions, literature data
GS11: Pelite, 8 GPa,1100°C
Mgs+ Arg+ L
L+Mgs+ K2Mg0.9Ca0.1
K2+ K2(Ca,Mg)ss
mol%
c. 1100°C, 6 GPa
GS11; Pelite, 8 GPa,1100°C
Dolss+L
Mgs+ Dol+L
Mgs+L
Mgs+K2Mg+L
K2Mg+L
K2+L
Mgss+K2Mgss
L
mol%
d. 1200°C, 6 GPa
GS11: Pelite, 5.5 GPa,1180°C
Dolss+L
K6Ca2+L
Mgs+L
K2Mg +L
Mgs+K2Mg+L
Mgss+K2Mgss
K2+L
B11: Lherzolite, 6 GPa,1200°C

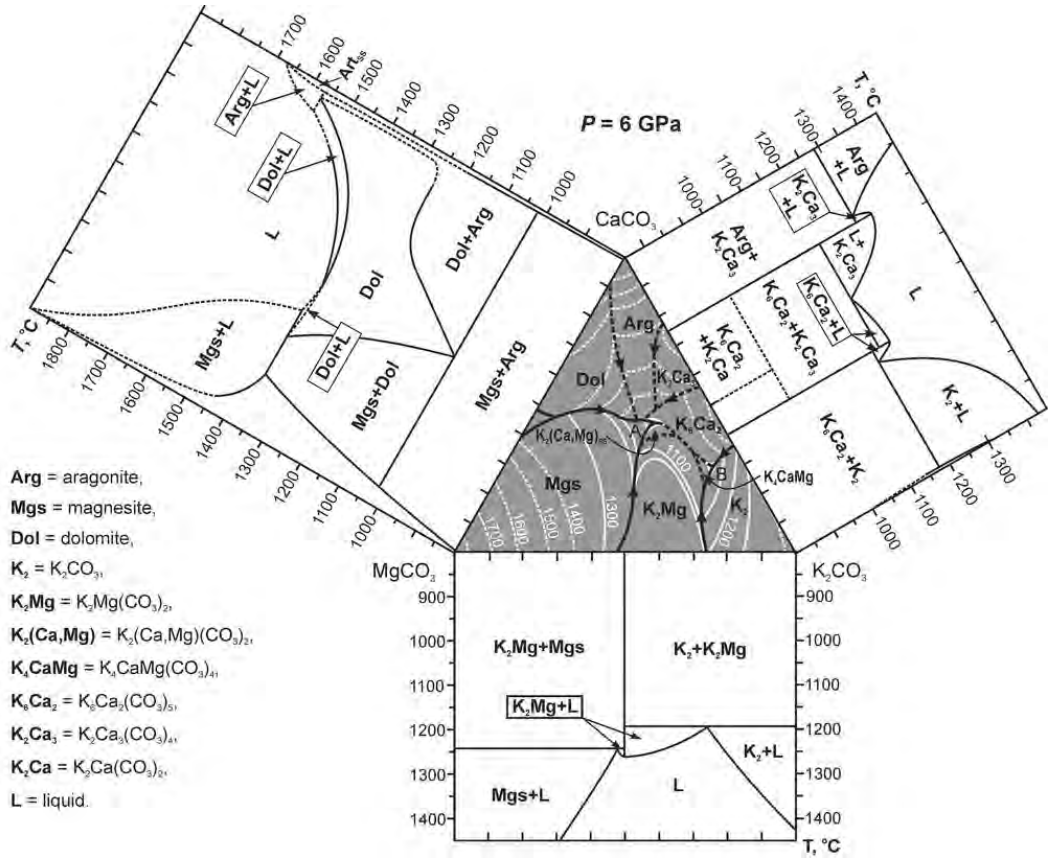

Arg = aragonite,
Mgs = magnesite,
Dol = dolomite,
K_2 = K_2CO_3,
K_2Mg = $K_2Mg(CO_3)_2$,
$K_2(Ca,Mg)$ = $K_2(Ca,Mg)(CO_3)_2$,
K_4CaMg = $K_4CaMg(CO_3)_4$,
K_6Ca_2 = $K_6Ca_2(CO_3)_5$,
K_2Ca_3 = $K_2Ca_3(CO_3)_4$,
K_2Ca = $K_2Ca(CO_3)_2$,
L = liquid.

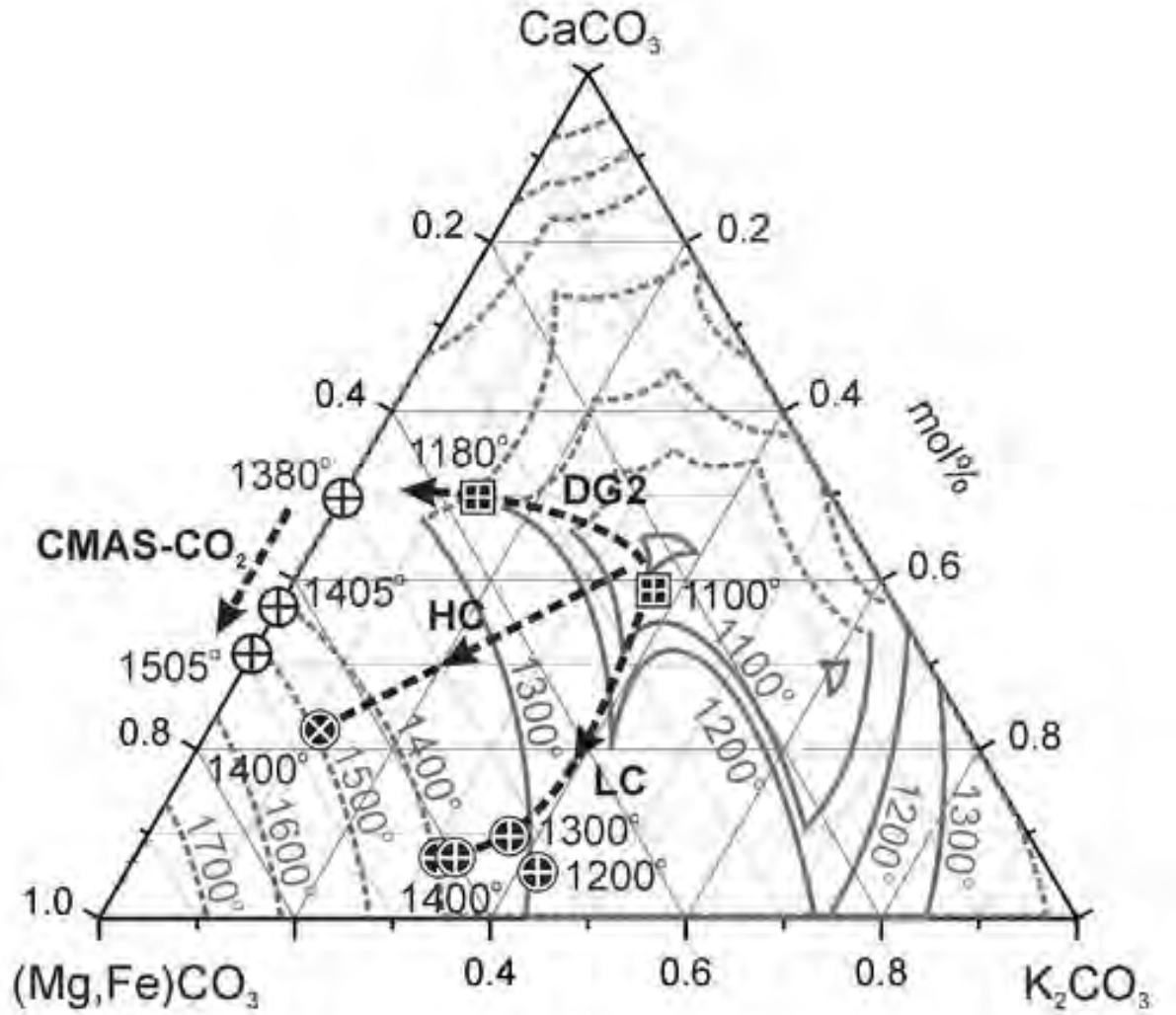

Partial carbonatite melt compositions:

⊕ DP98, **CMAS-CO$_2$** lherzolite, 6 GPa;

⊞ GS11, **DG2** Carbonated pelite, 8 and 5.5 GPa;

⊗ B11, **HC** harzburgite-K_2CO_3-$MgCO_3$, 6 GPa;

⊕ B11, **LC** lherzolite-K_2CO_3-$MgCO_3$, 6 GPa.

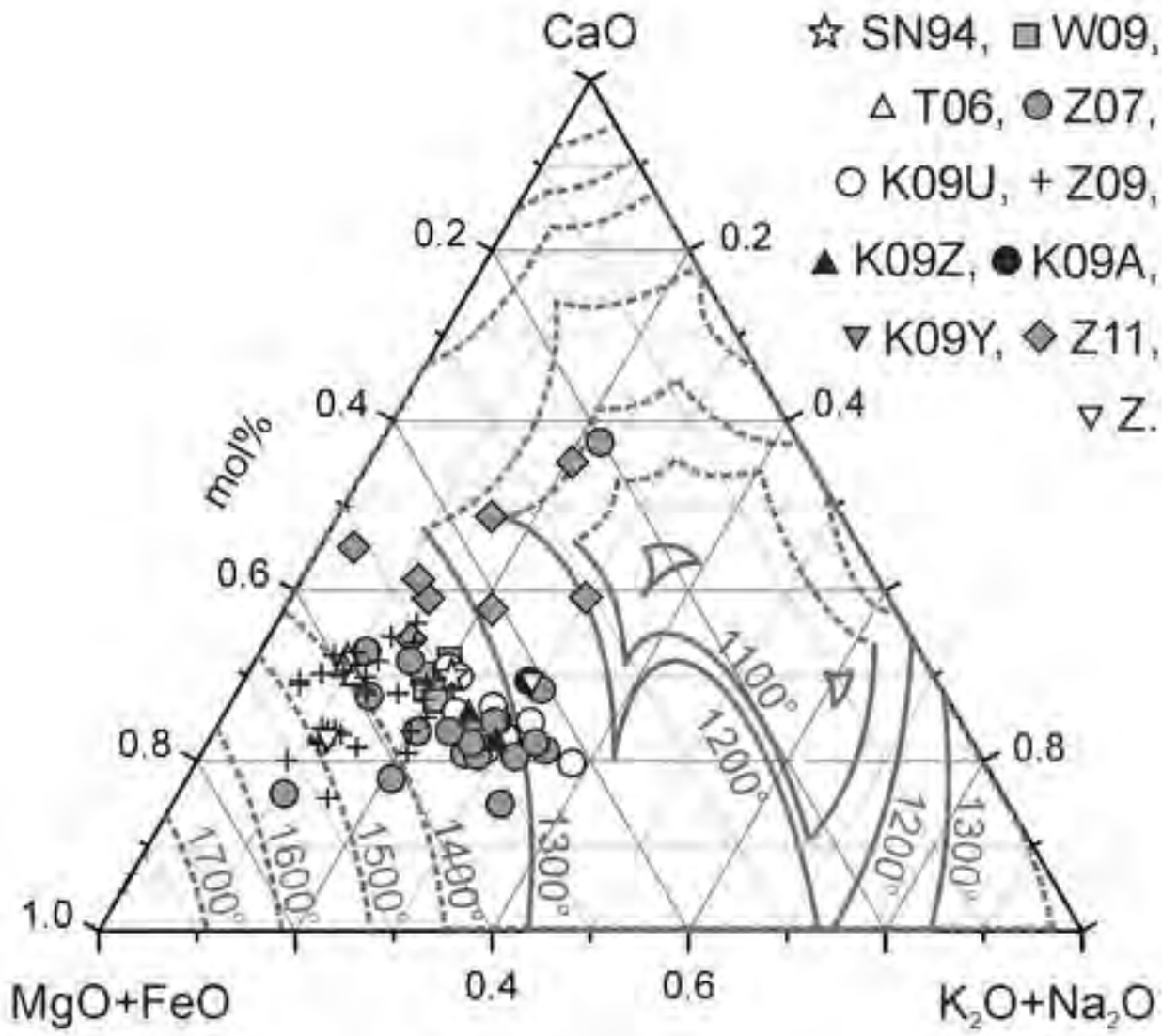
CaO
☆ SN94, □ W09,
△ T06, ● Z07,
○ K09U, + Z09,
▲ K09Z, ● K09A,
▼ K09Y, ◆ Z11,
▽ Z.
mol%
0.2
0.4
0.6
0.8
1.0
1100°
1200°
1300°
1200°
1300°
1700°
1600°
1500°
1400°
MgO+FeO
K_2O+Na_2O